

Event-based Continuous Color Video Decompression from Single Frames

Ziyun Wang¹, Friedhelm Hamann², Kenneth Chaney¹, Wen Jiang¹,
Guillermo Gallego², Kostas Daniilidis^{1,3}

¹University of Pennsylvania, USA.

²TU Berlin, ECDF Berlin and SCIOI Cluster, Germany. ³Archimedes, Athena RC

Abstract

We present **ContinuityCam**, a novel approach to generate a continuous video from a single static RGB image, using an event camera. Conventional cameras struggle with high-speed motion capture due to bandwidth and dynamic range limitations. Event cameras are ideal sensors to solve this problem because they encode compressed change information at high temporal resolution. In this work, we propose a novel task called **event-based continuous color video decompression**, pairing single static color frames and events to reconstruct temporally continuous videos. Our approach combines continuous long-range motion modeling with a feature-plane-based synthesis neural integration model, enabling frame prediction at arbitrary times within the events. Our method does not rely on additional frames except for the initial image, increasing, thus, the robustness to sudden light changes, minimizing the prediction latency, and decreasing the bandwidth requirement. We introduce a novel single objective beamsplitter setup that acquires aligned images and events and a novel and challenging **Event Extreme Decompression Dataset (E2D2)** that tests the method in various lighting and motion profiles. We thoroughly evaluate our method through benchmarking reconstruction as well as various downstream tasks. Our approach significantly outperforms the event- and image-based baselines in the proposed task. Please see our project website for code, data and additional results: https://www.cis.upenn.edu/~ziyunw/continuity_cam/.

1. Introduction

Temporally continuous videos are highly desirable for computer vision tasks because they allow an algorithm to avoid problems such as temporal aliasing and motion discontinuities. For example, correspondence becomes much easier if the temporal baseline between two frames is infinitely small. However, it is usually infeasible to acquire high-quality frames at high resolution. The bandwidth require-

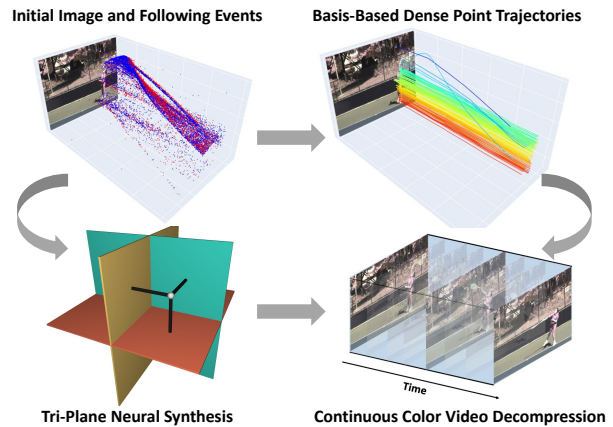


Figure 1. Event-based continuous color video decompression uses an initial frame and the events in a time window after the frame, to generate frames within the window. The prediction relies on a K-plane neural synthesis and a continuous trajectory field branch.

ment for high frame-rate videos grows proportionally to the frame rate. High-speed cameras often have hardware buffers that cache frames because large amounts of video data cannot be transferred in real time given the limited bandwidth of modern camera output interfaces. The root for this high bandwidth requirement can be attributed to the ubiquitous temporal redundancy in high-speed data. Modern camera sensors are designed to be synchronous, meaning that redundant information is given the same importance as more informative changes in pixels. Furthermore, the global shutter time of frame-based cameras assumes equal exposure of the entire frame, resulting in a limited dynamic range. These hardware limitations significantly increase the difficulties of capturing high-quality continuous videos.

A common solution to the problem is to learn motion interpolation networks to upsample videos by predicting intermediate frames. However, the interpolation task is inherently generative because many solutions exist between two sparsely sampled frames. State-of-the-art approaches produce only plausible middle frames based on hallucinated motions, which are usually assumed to be linear. These methods cannot reconstruct geometrically accurate frames

and suffer from common problems in upsampling such as aliasing. Reconstructing geometrically accurate frames cannot be solved simply with larger networks and more training data. This problem is illustrated in Figure 3.

We propose a novel solution to encoding high-speed video data by equipping the image sensor with a biologically inspired event camera. An event camera encodes the changes in log image intensity, outputting a stream of binary events that can be seen as a compressed representation of the image changes. Due to the sparse nature of events, the bandwidth requirement is significantly lower compared to traditional image sensors. These characteristics make event sensors ideal for capturing the subtle changes between frames, yet the question remains: what is the most effective way to unpack a video from static frames and dynamic events?

Brandli et al. [5] pioneered the research of high-speed video decompression, which decodes high-speed videos from events and APS frames from a DAVIS camera through direct event integration. Using direct integration to approximate the image signal suffers from noise and produces artifacts caused by discretization. Recent attempts have been made to use events to aid frame-based interpolation [55, 56]. However, these approaches depend on pairs of ideal regular frames that are susceptible to sudden degeneration caused by lighting changes and aggressive motions. For example, if the camera experiences a sudden drop or observes a sudden fast motion, the following frames would be corrupted, creating, thus, a blurry reconstruction. Additionally, since the interpolation needs to wait for the next frame, the latency for the prediction is much higher.

To enhance existing methodologies, we introduce a novel task called **event-based continuous color video decompression**. In this task, an initial color image and an aligned event stream are given, and the goal is to be able to query at any time within the event stream for a high-quality color image. Our approach features two method branches that directly encode long-term continuous videos. The first branch is K-plane-based neural synthesis, factorizing the continuous spatiotemporal feature into three feature planes. The design significantly reduces the computational burden of event voxelization. The second branch is a continuous trajectory field module that parameterizes dense pixel trajectories with a shared motion basis. The two branches are joined by a multiscale feature fusion network that flexibly generates frames at any desired timestamp. Additionally, we designed an open-source hardware-synchronized single-objective lens beam splitter for more precise data acquisition, which can facilitate the creation of hybrid image-event datasets. We developed a novel dataset tailored for the continuous color video decompression task. In addition to direct evaluation, we use the decompressed video in challenging downstream tasks such as Gaussian Splatting 3D recon-

struction and camera fiducial tag detection, even in difficult lighting and motion conditions. We summarize our contribution as follows.

- We propose the novel task of event-based continuous color video decompression from a single frame, aimed at addressing challenges in high-speed video acquisition.
- We present a novel approach to the proposed task via a joint synthesis and motion estimation pipeline. The synthesis module uses a K-plane-based factorization that encodes event-based spatiotemporal features. The motion estimation module estimates time-continuous nonlinear trajectories parameterized by a learned motion basis.
- We provide evaluation against various image- and event-based baselines, showing state-of-the-art performance.
- We contribute a novel event dataset using a meticulously designed beam-splitter setup with a shared-objective-lens design. In this dataset, we present various downstream 2D and 3D computer vision tasks, enabled by the video clips generated from our video decompression method.

2. Related Work

2.1. Video Decoding from Images

Frame interpolation methods focus on estimating missing information between low-frame-rate videos and inserting intermediate frames. Cheng et al. [7] adaptively learn separable convolution filters to sample more information pixels. FILM [43] warps a multi-scale feature pyramid to enable interpolation with large motion. FLAVR [23] uses spatiotemporal kernels to replace warping operations in flow-based VFI methods. AdaCof [27] combines kernel-based and flow-based modules to collaboratively predict interpolated frames. Niklaus et al. [37] proposed the use of Softmax splatting to replace image warping to achieve higher quality in occluded regions. Recently, TimeLens [55] and TimeLens++ [56] enhanced the VFI methods by introducing an aligned event camera. However, interpolation approaches are susceptible to sudden large motions and lighting changes. Our proposed method addresses this issue by eliminating the dependencies on a second frame. Additionally, our approach encodes long-range motion rather than small motion between every two frames.

Video prediction methods use previous frames to predict future frames. Due to the missing second frame, the dynamics of the scene need to be modeled and extrapolated into the future. Xue et al. [60] adopted a probabilistic framework for future frame synthesis, allowing multiple possible future frames to be generated. Lotter et al. [31] use Deep Predictive Coding Networks (DPCNs) to learn the structure of video data without manual annotation. Liu et al. [30] introduce a dense volumetric flow representation that produces coherent videos. Lee et al. [26] proposed using latent variational variable models and a generative ad-



Figure 2. Continuous long-term trajectory output on test sequences of BS-ERGB [56] dataset. The pixel tracks are computed using motion coefficients predicted from events. The tracked points are uniformly sampled from the first frame. We show only subsampled tracks, but the network outputs dense tracks in a single feedforward pass. The color indicates a spatial coordinate. Our continuous basis-enabled motion module can decode complex long-range motion from events. Best viewed in color.

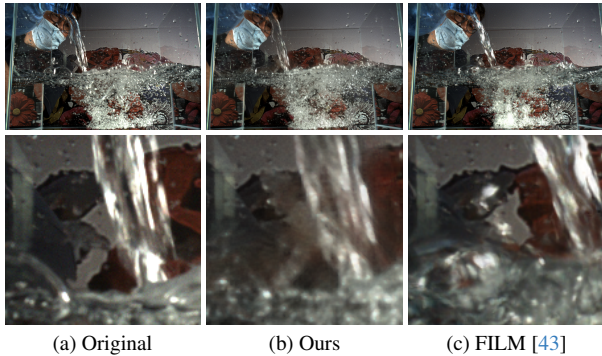


Figure 3. Original (a), Predictions from our method (b) and state-of-the-art video interpolation (c). Video interpolation cannot recover highly non-linear motion between two frames. Our method uses continuous event information to recover the true scene.

versarial framework to achieve diversity and quality. More recently, DMVFN [20] used a differentiable routing module to perceive the motion scales of a video. Due to the increasing quality of generative models, a new line of research arises for unguided video synthesis from a single image [10, 17, 19, 28]. This line of methods does not focus on accurate geometry, but rather on perceptual quality and diversity.

2.2. Event-based Motion Estimation

Event data have been shown to be suitable for fine motion estimation due to their high temporal resolution and relative invariance to light changes [2, 12, 14, 62, 67]. Early work has focused on the computation of asynchronous optical flow, which is based on the fitting of the plane in the spatiotemporal domain or the approximate gradient of events [2, 3]. Subsequently, data-driven techniques have been suggested to enhance the dependability of flow com-

putation in the presence of noise in event streams. Zhu et al. [66] suggest a self-supervised method for learning flow by warping consecutive pairs of images. Gallego et al. [12] formulate the flow estimation problem as maximizing the contrast of flow-warped events. This technique is then extended to more tasks such as unsupervised visual odometry [67], depth estimation [65, 67], and motion segmentation [52]. Contrast maximization requires only events, but it is challenging to optimize the contrast loss directly. Therefore, a recent corpus of literature focuses on “taming” this loss function with additional regularization [49, 50]. In addition to creating more effective loss functions, several recent supervised studies have improved architecture designs to enhance the general performance of the model [14]. However, the proper representations to understand long-range motion remain understudied. Gehrig et al. [15] and Tulyakov et al. [56] use B-splines to parameterize the trajectory of points. Both methods use intermediate image frames as input to the network in addition to events to improve photometric consistency in motion estimation.

2.3. Event-based Video Reconstruction

Reconstructing intensity information from event cameras has been approached through two primary methodologies: filtering and learning-based techniques. Initial efforts concentrated on developing suitable filters for sparse event signals. These filtering methods typically involved classical strategies such as integration [45] or reconstructing through intermediaries like gradients and Poisson Reconstruction [25]. However, these approaches were often plagued by noise and event leakage at corners. A notable advancement was the incorporation of optical flow to improve image reconstruction [1]. An effective strategy addressing the offset issue in these methods is the direct mea-

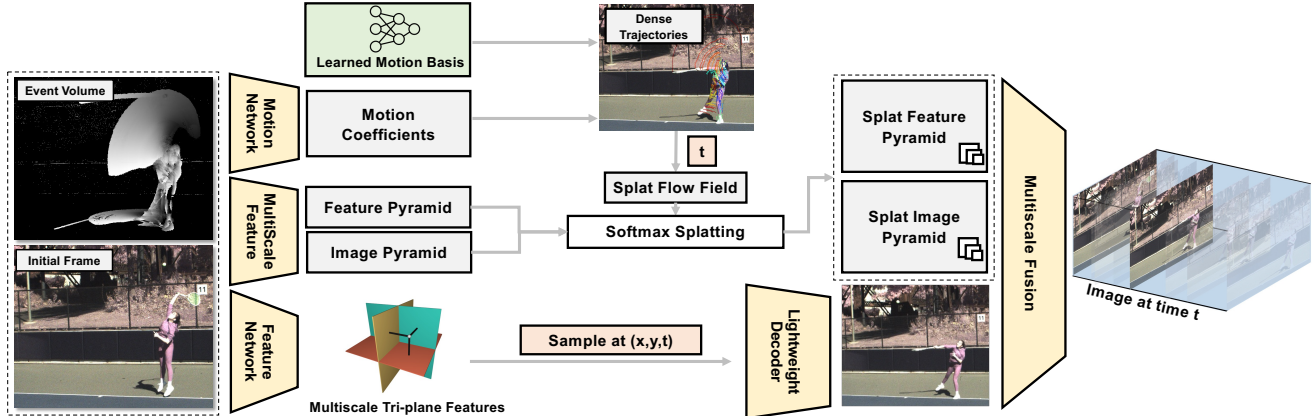


Figure 4. *Pipeline*. The pipeline of ContinuityCam has two branches. The initial frame and the long range event volumes are concatenated forming the network input. **Top**: A continuous motion network regresses the motion coefficients for generating the point trajectory for every pixel from events and the initial frame. Then the multiscale features are forward-splatted to a future time. **Bottom**: The input is projected to a set of three feature planes. A lightweight decoder queries the feature tri-planes and decodes the synthesized pixel RGB values. Finally, the two branches are merged by a multiscale feature fusion network into a final high-quality frame prediction.

surement with an image sensor, followed by the application of a complementary filter [45] adjusting the offset for each pixel.

In contrast, learning-based methods have demonstrated the ability to surmount many of these challenges. By embedding priors within the models, they generate realistic images solely from event data [41, 42, 59]. Furthermore, these approaches have been extended to incorporate images into the input data stream, enhancing the production of high dynamic range images [61]. Efficient image generation is also achieved through shallow networks, either via recurrent networks [46] or through intermediary networks coupled with traditional post-processing techniques [9, 64].

Complementary to these methods, other asynchronous sensors offer grayscale estimation through timing information. The ATIS sensor, for instance, emits a spike after the initial event, with timing proportional to the grayscale level. Similarly, the Vidar One [6] operates by transmitting spikes at a frequency corresponding to the grayscale level of each pixel. These innovative features enable accurate grayscale level determination in moving scenes using the ATIS and even in static scenes with the Vidar One [21].

3. Method

3.1. Continuous Event-based Trajectory Field

To model long-range motions, one needs to carefully choose the motion representation. Naively, flow defined on discrete steps can be directly regressed from a motion network. However, the problem with this formulation is that the motion is completely unconstrained and does not exploit the temporal smoothness of the pixel trajectories. Motion priors in terms of motion basis have been proposed to address this issue in 3D dynamic motion modeling [28, 29, 57]. For

a set of points $X_0 = \{x_0 \dots x_N\}$ defined at beginning of the video, and a set of basis values defined on frame timestamps $\theta_T = \{\theta_0 \dots \theta_T\}$, the trajectory of N points can be modeled by multiplying the motion coefficients per point $\alpha(x_i)$ and the corresponding basis values. This is usually modeled by a matrix multiplication:

$$\mathbf{X} = [x_i(t_j)]_{i=0,\dots,N;j=1,\dots,T} \quad (1)$$

$$\mathbf{\Lambda} = [\alpha_l(x_i)]_{i=0,\dots,N;l=0,\dots,K} \quad (2)$$

$$\mathbf{\Theta} = [\theta_{m,t_j}]_{m=0,\dots,K;j=1,\dots,T} \quad (3)$$

where $\mathbf{X} \in R^{N \times T}$, $\mathbf{\Lambda} \in R^{N \times K}$ and $\mathbf{\Theta} \in R^{K \times T}$. The motion trajectory of a set of points is obtained by: $\mathbf{X} = \mathbf{\Lambda} \mathbf{\Theta}$. The matrix $\mathbf{\Theta}$ is a set of shared parameters that do not depend on input during inference. However, this formulation does not allow for querying arbitrary time. Specifically, the matrix $\mathbf{\Theta}$ is still fix-sized. Due to the continuous nature of events, we propose to represent the continuous trajectory field of the events using a continuous-time function. We replace the discrete matrix $\mathbf{\Theta}$ with a set of learned basis functions $\Omega = \{g_k^\theta(t)\}$ where $t \in R$, $|\Omega| = K$. This continuous formulation allows the network to map continuous motion information of events to continuous trajectories. Specifically, at time t , an initial point x_i is observed at y_i where $y_i(t) = \sum_{k=1}^K \alpha_k(x_i) g_k^\theta(t)$. The selection of a motion basis offers several possibilities, including the Discrete Cosine Transform [29, 57], Fourier basis [28], and polynomial basis. In our experiments, the hand-crafted basis tends to be dependent on carefully chosen hyperparameters, such as the frequency band. To address this, we employ a learned MLP to model the motion basis and optimize it during training. The number of basis functions is correlated with the motion complexity of the video clips. Specifically, for the two main datasets that we primarily study, we use $K = 5$, shared be-



Figure 5. Qualitative Evaluation: We present two qualitative examples from E2D2 and BS-ERGB [56], respectively. Our method, ContinuityCam, demonstrates enhanced accuracy in reconstructing geometry, even with challenging deformable subjects, such as in the “Fire” sequence (Column 4). This improvement is attributed to the effective use of event data. Notably, in low-light conditions, as seen in the “Gnome” sequence, our approach markedly reduces motion blur compared to traditional image acquisition methods. While FILM [43] generates plausible results, it fails to accurately predict geometry in all examples. DMVFN [20] struggles with occlusions, particularly those caused by rotational movements, as evident in the “Gnome” sequence.

tween $x(t)$ and $y(t)$. Figure 2 illustrates the sample trajectories predicted by our method on the BS-ERGB [56] data set. It can be seen that our method captures complex non-linear motion over a long-range event window.

3.2. Event-based K-Planes for Neural Synthesis

A major limitation of warping-based methods is occlusion handling. Pixels that are not seen in the first frame cannot be accurately recovered, ubiquitously observed with a moving camera. In video interpolation methods, this problem is addressed by providing the next frame, which often already contains the occluded pixel. However, we do not have this privileged information from the future. To address this issue, we turn to events for more pixel-level information about the occluded areas. Events provide more than just the optical flow information used for warping. Rather, directly integrating events with the previous image as the initial condition provides strong cues for occluded regions. Here we describe the relationship between $L(t)$, the frame to be reconstructed, L_{t_0} , an initial frame, and Γ , the set of events from time t_0 to t .

Letting the event field be a function of continuous time t

such that an event $e_k = (\mathbf{x}_k, t_k, \sigma_k)$, with $\mathbf{x}_k = (x_k, y_k)^\top$, is represented by $e_{\mathbf{x}}(t) = \sigma_k \delta(t - t_k)$ [45], we may write $E(0, t)$, the brightness change between 0 and t at pixel \mathbf{x} by $E_{\mathbf{x}}(0, t) = \int_0^t e_{\mathbf{x}}(s) ds \approx \sum_{e_i \in \hat{\Gamma}_{\mathbf{x}}} \sigma_i$, where $\hat{\Gamma}_{\mathbf{x}}$ denotes the discrete set of events at a pixel \mathbf{x} in $[0, t]$. Based on the event generation model [34, p. 3], a frame L at the time t can be written as $L(\mathbf{x}, t) = L(\mathbf{x}, 0) \exp(cE_{\mathbf{x}}(0, t))$ where c is the contrast threshold/sensitivity.

Why does direct integration fail? It can be seen that this formulation requires that the contrast threshold of the integration is known and that both the initial frame and the reconstructed frame are assumed to be perceived by the same mapping function between the physical light and pixel value. Unfortunately, neither is the case for this task. The contrast threshold c cannot be easily obtained with existing large-scale datasets [45]. Furthermore, the sensor characteristics of the aligned RGB and event sensors do not share the same mapping between the physical light and the pixel value. Techniques such as gamma correction need to be applied to recover a visually pleasing reconstruction [44]. Noise [13, 39] and contrast imbalance [39] also present major challenges in accurate integration.

Event-based K-Plane Features. Encoding a continuous video requires the ability to query an image at a high temporal resolution. To make high-speed video generation computationally feasible, the synthesis operation should be done once for each video, and the sampling operation at each step should be comparatively cheap. Therefore, we adopt a novel K-Planes parameterization for a reconstructed video. Specifically, we assume that the characteristics are encoded on three orthogonal planes denoted by P_{xy} , P_{xt} , and P_{yt} . These three planes contain the feature information for the continuous video field on discretized grids. For dense video, we ensure that the resolution of the time dimension in P_{xt} and P_{yt} is sufficiently large for fine-grained temporal information. This significantly reduces the feature dimension from three-dimensional to two-dimensional. Then a lightweight decoder ϕ is used to decode the three feature vectors to the RGB value. Formally, given a spatiotemporal coordinate $\mathbf{q} = (x, y, \tau)$, the decoded image value can be written as:

$$f(\mathbf{q})_k = \phi(P_k(\pi_k(q))), \quad (4)$$

where π_k denotes the operation that maps a three-dimensional point q to its corresponding position in Plane k . We use a multiscale feature extractor to directly regress the three planes at three spatial dimensions. Following K-Planes NeRF [11], we use Hadamard product to fuse features of different planes at each scale.

A key benefit of using such a parameterization is that it shifts the computational cost to the encoder to reduce the cost of sampling. Our synthesis encoder runs once to reconstruct a short video clip, whereas the lightweight decoder can query with little computational cost. Furthermore, we no longer need to make a different event volume for every inference, compared to the synthesis models in TimeLens++ [56].

3.3. Latent Frame Flow Refinement

In Sec. 3.1, we introduce a novel long-range motion model supported by a learned basis. The continuous flow field captures the long-range motion within events. However, there is significant noise in the event-based flow field caused by noisy measurement and areas that do not have enough contrast to generate events. Therefore, it is critical to learn the grouping of the flow field for spatially consistent warping. To this end, we propose a novel latent frame model that takes advantage of the iterative matching power of frame-based flow networks.

In Sec. 3.2, we describe how an intermediate latent frame can be obtained through our neural event integration module. We use this latent frame for computing the latent frame flow via iterative flow refinement. Given a latent frame flow via iterative flow refinement. Given a latent frame $\hat{I}(t)$ and an initial frame I_0 , we build a correlation pyramid based on the features of the image $F((\hat{I}_t))$ and $F(I_0)$. Following

	Events	PSNR \uparrow	LPIPS \downarrow	SSIM \uparrow
Two-frame Interpolation Methods				
TimeLens [55]	✓	20.62	0.230	0.674
FILM [43]	✗	28.16	0.055	0.798
Single-Frame Decompression Methods				
E-RAFT unrolling	✓	17.19	0.257	0.583
E-RAFT (inpainted)	✓	19.58	0.260	0.623
RAFT unrolling	✗	19.35	0.197	0.629
RAFT (inpainted)	✗	20.88	0.222	0.659
DMVFN [20]	✗	25.93	0.111	0.767
Ours	✓	28.68	0.077	0.802

Table 1. Video Reconstruction Comparison on our dataset. In addition to the image-based video prediction results, we show interpolation methods for reference.

RAFT [54], we produce correlation volumes at each step:

$$C(F((\hat{I}_t))_{i,j}, F(I_0)_{k,l}) = \sum_h F((\hat{I}_t))_{i,j,h} F(I_0)_{k,l,h}, \quad (5)$$

where i, j, k, l are the spatial coordinates of the features, and h is the feature index. At each step m , the network takes the images and the correlation volume at each scale and iteratively produces an update to the previous update $\delta_m(t)$ to the previous displacement $\Delta_{m-1}(t)$. Finally, the flow prediction at step m is $\Delta_m(t) = \Delta_{m-1}(t) + \delta_m(t)$.

The correlation volume in (5) resembles a matching process without a motion model, allowing matching at any two arbitrary time steps. A key factor that motivates the choice to use this latent model is the empirical observation that the correlation function $C(F((\hat{I}_t))_{i,j}, F(I_0)_{k,l})$ is robust to color changes and noisy images. The neural synthesis module in Sec. 3.2 produces images that are inaccurate in color due to missing information. However, these latent frames show enough texture features for RAFT to build meaningful correlation modules for matching. To reduce the training burden, we directly use the RAFT weights pre-trained on FlyingChairs [8] and FlyingThings3D [33].

3.4. Multi-scale Feature Fusion

In the previous section, we introduced three main outputs of the network. The motion module produces a set of continuous point trajectories (Sec. 3.1). The event-based neural integration model synthesizes a rough reconstruction of a target frame (Sec. 4.1). The latent flow refinement module produces a texture-based motion field based on global correlation (Sec. 3.3). We fuse these outputs via a multiscale feature fusion network. For the sake of simplicity, we remove the subscript of the point index in all symbols. We denote $M(t)$ as the long-range flow (offset) of a point at time t , $\tilde{M}(t)$ the latent flow, $\Psi(I_0)$ a feature pyramid computed from the starting frame I_0 , and $\mathcal{P}(I_0)$ an image pyramid computed from I_0 . In addition, we define the forward

	Events	skip 1		skip 3	
		PSNR \uparrow	LPIPS \downarrow	PSNR \uparrow	LPIPS \downarrow
Two-frame Interpolation Methods					
FLAVR	\times	25.95	<i>0.086</i>	20.90	<i>0.151</i>
DAIN	\times	25.20	<i>0.067</i>	21.40	<i>0.113</i>
SuperSlowMO	\times	-	-	22.48	<i>0.115</i>
QVI	\times	-	-	23.20	<i>0.110</i>
FILM [43]	\times	25.09	0.066	22.91	0.086
TimeLens [55]	\checkmark	28.36	<i>0.026</i>	27.58	<i>0.031</i>
TimeLens++ [56]	\checkmark	28.56	<i>0.022</i>	27.63	<i>0.026</i>
Single-Frame Decompression Methods					
DMVFN [20]	\times	22.63	0.218	21.11	0.250
E-RAFT unrolling	\checkmark	19.28	0.171	17.49	0.257
E-RAFT (inpainted)	\checkmark	20.40	0.160	18.79	0.222
RAFT unrolling	\times	22.85	0.120	20.88	0.197
RAFT (inpainted)	\times	23.41	0.097	20.88	0.142
Ours	\checkmark	25.40	0.088	24.80	0.095

Table 2. Video Reconstruction Comparison. In addition to the image-based video prediction results, we show interpolation methods for reference. (LPIPS values in italic were reported in TimeLens++ [56]. The metric implementation might differ from ours.)

splatting function $\mathcal{T}(\cdot)$, $\mathcal{C}(\cdot)$ as a pyramid concatenation operation. We splat multiscale features and image pyramids with the two flows. The input to the fusion model reads

$$\mathcal{G} = \mathcal{C}\left(\mathcal{T}_{M(t)}(\Psi(I_0)), \mathcal{T}_{M(t)}(\mathcal{P}(I_0)), \mathcal{T}_{\tilde{M}(t)}(\mathcal{P}(I_0)), \mathcal{T}_{\tilde{M}(t)}(\Psi(I_0)), \mathcal{P}(\hat{I}_t)\right) \quad (6)$$

The final image prediction is passed through the multi-level merging network f_m , implemented by a series of convolution layers with small receptive field and non-linear activation, to produce the final prediction $\hat{Y} = f_m(\mathcal{G})$. We use Softmax Splatting [36] to warp images and features at each pyramid scale, with learned multiscale splatting weights predicted along with motion parameters. The splatting shows instability for flow supervision, so the gradient of the flow input to the splatting operation is stopped.

3.5. Loss Functions

Optical Flow Loss We use two approaches for supervising the predicted continuous optical flow field: self-supervised and supervised. We adopt the image-based warping loss proposed in EVFlowNet [66]. This allows the network to learn flow solely based on photometric consistency. Given the forward flow displacement computed from the motion network, we bilinearly sample image I_t based on the backward warp field to $t = 0$. We write the warping operation as $\hat{I}_{\text{warp}} = \mathcal{B}_{\tilde{M}(t)}(I_t)$. The warping loss comprises a photometric loss L_{photo} and a smoothness loss L_{smooth} .

$$L_{\text{photo}}(I_0, \hat{I}_{\text{warp}}) = \rho(I_0 - \hat{I}_{\text{warp}}; \beta) \quad (7)$$

where $\rho(\cdot)$ is the Charbonnier loss function $\rho(x) = (x^2 + \epsilon^2)^\beta$. The smoothness loss regularizes the flow field to avoid the aperture problem in the classical flow estimation problem. We use second-order smoothness L_{smooth} , which is the norm of the gradient of the image gradient. For supervised loss, we compute the L1 loss between the predicted displacement $M(t)$ and the image-based flow W_t computed from RAFT [54], the L1 flow loss is:

$$L_1(M(t), W_t) = \|M(t)_i - W_t\|_1 \quad (8)$$

The supervised loss helps the network learn longer-term consistency since the pseudo ground truth RAFT flow is computed using correlation-based matching. Moreover, it helps the network learn to infer dense flow events in places without events, due to the limited contrast. RAFT flow helps group pixels that have similar motion. Although supervised loss provides a direct motion signal, the pre-trained image-based flow suffers from aliasing and missing details. Therefore, we use self-supervised flow to help further correct the flow by computing photoconsistency loss directly on image sensor measurement.

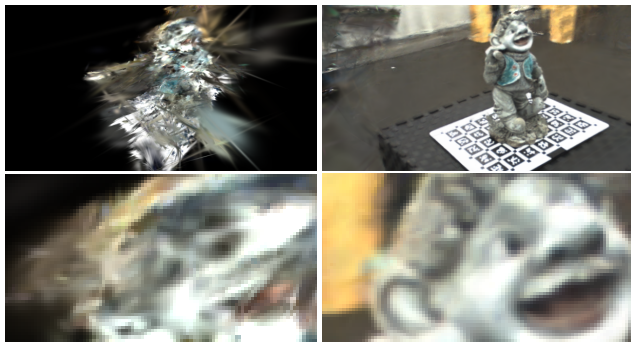
Image Reconstruction Loss Our approach employs a composite loss function, combining L1 loss with Perceptual loss [22], to harness their respective strengths. The L1 loss enhances the accuracy of each pixel, while the Perceptual loss increases the clarity and realism of the result. Given reconstruction \hat{Y} and image ground truth Y , $L_1(\hat{Y}, Y) = \|\hat{Y}_i - Y_i\|_1$ and $L_p(\hat{Y}, Y) = \frac{1}{J} \sum_{j=1}^J |\phi_j(\hat{Y}) - \phi_j(Y)|_1$ where $\phi_j(\cdot)$ is the deep features extraction operator, utilizing a backbone VGG-19 network at level j . We weigh these two losses equally. The joint loss is computed on both the event-based neural synthesis results and the final output.

4. Experiments

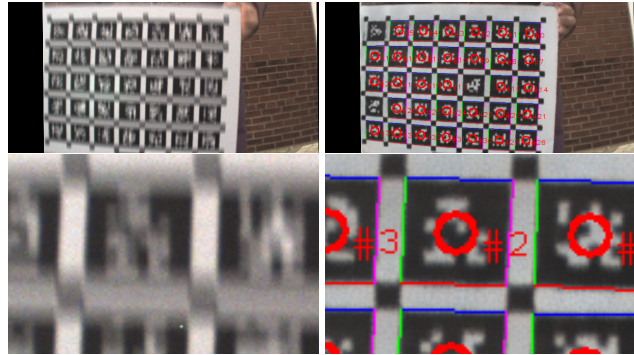
We evaluate the reconstruction quality of Continuity-Cam on BS-ERGB [56] and our newly developed dataset E2D2. In these experiments, we use Peak-Signal-to-Noise-Ratio (PSNR), Learned Perceptual Image Patch Similarity (LPIPS) [63], and Structural Similarity (SSIM). However, in most cases, events are useful when the scene experiences sudden changes. Therefore, we use our carefully designed beam splitter set-up to curate additional scenes with challenging conditions. In Section 4.1, we show direct photometric results with high-quality images. In Section 4.2, we show how our method can generate blur-free Gaussian Splatting and detect fiducial tags more robustly.

4.1. Video Reconstruction Evaluation

For quantitative evaluation on BS-ERGB [56], we follow the evaluation scheme of TimeLens. We take keyframes that are 1 and 3 frames apart and predict the skipped frames. For evaluation on E2D2, we use a predicted time to 0.25s rather than a fixed number of frames because the amount of



(a) 3D Gaussian Splatting reconstruction improves with the use of the decompressed images.



(b) AprilTag detection at the same moment in time. The detection rate increases from 0 to 32 detections by decompressing images using events.

Figure 6. Qualitative downstream applications comparing original blurry frames (Left in each sub figure) to the decompressed frames (Right in each sub figure). Each is shown with a full image and zoomed in to show detail beneath.

motion for a given scene is correlated to duration and invariant to camera frame rate. The frame rate of our dataset ranges from 10 to 66 Hz, resulting in 2 to 17 skipped frames. E2D2 has four splits: Train, Validation, Quantitative Test and Qualitative Test. The qualitative test set contains scenes with mostly motion-blurred images, which do not have sharp ground truth. We provide metrics evaluated on the quantitative test set with 4686 frames. We provide the following additional baseline methods: **Frame Interpolation.** We use FILM [43] for direct interpolation between two keyframes. **Video Prediction.** DMVFN [20] predicts a frame based on the previous two frames. We predict a video iteratively by treating predicted frames as input to the next prediction. **Flow Unrolling.** In this class of baseline methods, a frame is iteratively warped forward in multiple steps using the backward optical flow using RAFT [54] and E-RAFT [14] respectively. **Inpainted Flow unrolling.** For both flow unrolling methods, we additionally refine the predictions by training a U-Net to reconstruct the original frames from the intermediate (flow unrolling) predictions.

The evaluation results on BS-ERGB [56] and E2D2 are shown in Table 2 and Table 1 respectively. Two-frame interpolation methods use the keyframe before and after an evaluated frame. Single-frame decompression methods use only the previous key frame. The task is considerably harder as there is no information about occlusion regions in the initial frame. Nonetheless, ContinuityCam outperforms all single-frame decompression methods by a large margin on both datasets. Our method achieves the best score on E2D2 and beats all frame-only methods on BS-ERGB. Our research demonstrates that ContinuityCam has more advantages when applied to E2D2, as evidenced by the qualitative results in Figure 5, which demonstrate that interpolation methods are vulnerable to corrupted second frames.

4.2. Downstream Applications

Blur-free Gaussian Splatting 3D reconstruction has long been a task that has achieved varying results with traditional images. It is also a task commonly plagued by non-ideal input images (e.g. blurry images). Camera pose estimation and calibration are achieved by running COLMAP [47, 48] for the original images and our decompressed images separately. These results are used to reconstruct the 3D scene with 3D Gaussian Splatting [24]. Figure 6a shows the final results with ContinuityCam providing significantly sharper reconstructions.

Fiducial Tag Detection AprilTags [38] represent an external validation of the geometric consistency of our reconstruction at a fine-grained resolution. Each tag is detected through the high-contrast square and decoded through the bit pattern on the interior. This AprilTag grid is commonly used in calibration pipelines [32] or as robust SLAM features [40]. For these tasks, many detections are required. We see an improvement in detection rate from 8,854 detections in the original imager to 10,342 with ContinuityCam (an improved detection can be seen in Figure 6b).

5. Conclusion

In this work, we introduce ContinuityCam, a novel method for the event-based continuous color video decompression task, using a single static RGB image combined with event camera data. The core of the method is founded on two novel representations for both the photometric changes and the pixels' motions predicted from events. Our approach does not rely on additional frames except for the initial image, enhancing robustness to sudden lighting changes, minimizing prediction latency, and reducing bandwidth requirements. We thoroughly evaluate our method on existing datasets and our carefully crafted dataset, E2D2, showing state-of-the-art performance in event-based video color video decompression. Additionally, we showcased practical

applications of our method in various scenarios, including 3D reconstruction and camera fiducial tag detection, even under challenging lighting and motion conditions.

Acknowledgment: We gratefully acknowledge the support by the following grants: NSF FRR 2220868, NSF IIS-RI 2212433, NSF TRIPODS 1934960, ONR N00014-22-1-2677, the Deutsche Forschungsgemeinschaft (DFG, German Research Foundation) under Germany’s Excellence Strategy – EXC 2002/1 “Science of Intelligence” – project number 390523135 and the NSF AccelNet NeuroPAC Fellowship Program. We thank Jiayi Tong for help with visualization and proofreading.

Event-based Continuous Color Video Decompression from Single Frames

Supplementary Material

Section 1 provides implementational details of our and the baseline methods. Section 2 presents more details on E2D2 and our camera setup.

1. Implementation Details

In this section, we provide full details of the proposed architecture (Sec. 1.1), specifics of the training (Sec. 1.2), a discussion of the input representation (Sec. 1.3), and lastly details on the implementation of the baseline methods (Sec. 1.4).

1.1. Model

K-plane Synthesis Network The K-plane synthesis network has three components: feature encoder, K-plane sampler, and pixel color decoder. The feature decoder is implemented as a U-Net with 4 encoders, 2 residual bottleneck layers, and 4 decoders, with skip connections. The U-Net backbone is depicted in Figure 7. The feature encoder maps the input event volumes and an initial image to a 24 channels, 8 for each plane. The K-plane sampler uses bilinear sampling to query features at a given x, y, t coordinate. The queried features are concatenated and fed into a final pixel color decoder. The pixel color decoder can be implemented using either a lightweight MLP or a lightweight CNN. For our task, we often care about a whole image rather than individual pixels. Therefore, we deployed an efficient three-layer CNN decoder, with each hidden layer having 64 kernels and ReLU activation, to decode image pixel color.

Motion Basis Network The motion basis network is a MLP network that maps a single scalar time value to a set of query values. This network is shared between **all** instances, which means that it is not conditioned on the input of events and images into the network. We use it as a set of query-able, time-continuous functions. The network has two hidden layers with 64 neurons and ReLU activation functions. The network outputs 5 values which are the output of 5 basis functions. The function values are also shared between x and y trajectories. The x and y trajectory coefficients are predicted separately per-pixel, as detailed in the next section.

Motion Trajectory Field Network The motion trajectory network is based on the same backbone as the K-plane synthesis branch, as described in Figure 7. The network predicts $(K \times 2 + 1)$ channels. The first $2K$ channels are the motion coefficients for x and y trajectory separately. The last channel is the splatting weight for the Softmax splatting

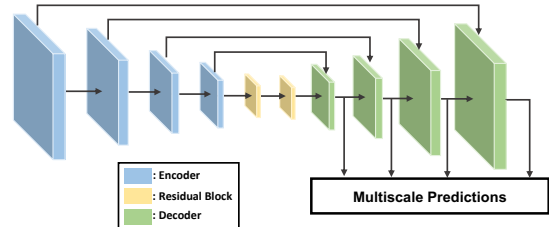


Figure 7. Backbone architecture. The U-Net with skip connections maps event volumes and images into multi-scale dense output.

operation. We use Tanh activation for the softmax weight to improve the numerical stability of the Softmax function.

Multi-scale Feature Fusion Networks We include the network architecture of our multiscale feature fusion network in Figure 9. The warped features at different scales are upsampled to the nearest-neighbor method. The features are then fed through a series of convolutional layers. By doing this iteratively, we gradually fuse the multi-scale image and feature pyramids in a course-to-fine fashion.

1.2. Training

We train the K-plane synthesis network and the motion network separately and jointly optimize a shared feature fusion network to fuse the two branches.

For the K-plane synthesis network, we use a learning rate of 10^{-4} with an Adam optimizer. We train the network for 20,000 iterations. We separately train the motion network to predict pixel trajectories, supervised with a image warping loss and L1 flow loss described in Section 3.5. Additionally, we train a dummy feature fusion network to map the warped image features and dummy synthesized frames to a final prediction. Here, we do not have the latent frame flow for warping features. The key idea is to train the network to rely only on events to estimate motion trajectories. The network is trained for 15,000 iterations with a learning rate of 10^{-4} with an Adam optimizer. We directly use FILM's [43] pre-trained multi-level feature encoder without fine-tuning.

In the end, we take the trained K-plane synthesis network and motion network and fuse their predictions with a multilevel feature fusion network. In this final training, we insert the warped features according to the latent frame flow as described in Section 3.3. We jointly optimize all parts of the network except the frozen image encoder. The entire network is trained 100,000 steps with the same learning rate and optimizer configuration as the motion network.

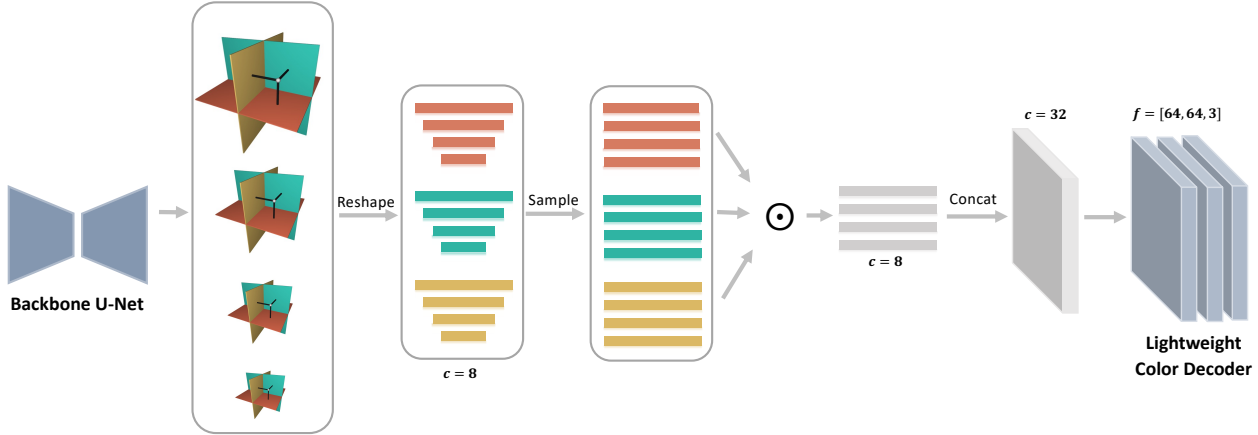


Figure 8. The architecture for the K-planes synthesis module. The initial image and event volume are mapped to multi-scale Tri-planes (xy, xt, yt). These feature planes are sampled bilinearly and fed into a lightweight color decoder network.

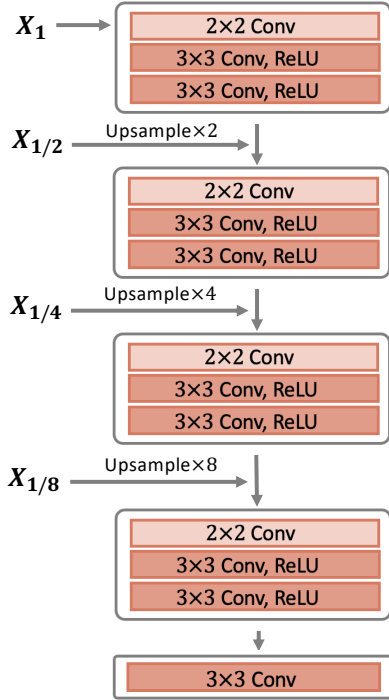


Figure 9. Architecture for the multi-scale feature fusion network. The warped feature and image pyramids are gradually injected into the network via a series of upsampling and convolution.

We design the training process to maximize the information learned in the K-plane synthesis network and the motion network. For data augmentation, we randomly perform flipping along the x and y directions, randomly rotate at $[0, 90, 180, 270]$ degrees, and then randomly rotate between

$(-45, 45)$ degrees.

1.3. Input Representation

We use an event volume similar to EvFlowNet [66]. For a set of events $\Gamma = \{(x_i, y_i, t_i, p_i)\}$, an event volume $E(x, y, t)$ containing these events is written as

$$E(x, y, t) = \sum_i p_i k_b(x - x_i) k_b(y - y_i) k_b(t - t_i), \quad (9)$$

where $k_b(\cdot)$ is a bilinear sampling kernel function. We used 60 temporal channels to encode events into spatio-temporal volumes. A large number of input channels is selected because we encode the long-range event motion. For the event-based motion network, we normalized the event volume to have a maximum of 1 and a minimum of -1 because the network flow should be invariant to the absolute number of events in the volume. For the synthesis branch, we do not normalize because the pixel-wise change should vary with respect to the number of events. We separated positive and negative events and concatenate the volumes together because of the asymmetric contrast threshold. Positive and negative events cannot be canceled out by each other due to the unknown ratio between the two contrast thresholds.

1.4. Baselines

This section provides additional information to the baseline methods.

Frame Interpolation. We use FILM [43] for direct frame interpolation between two key frames. This method does not use event data and relies on the key frame before and after the desired generated frame.

Video Prediction. DMVFN [20] performs video prediction. The model takes two consecutive frames and predicts the next one. We predict the hold-out frames after a

key frame, in an iterative manner, starting with a key frame and the original frame before the key frame.

Flow Unrolling + RAFT. In this method, the frame is iteratively warped forward in multiple steps using optical flow, which is determined using RAFT [54]. To allow the warping frame f_i to f_{i+1} , we determine the backward flow from t_{i+1} to t_i , using the original frames (ground truth).

Flow Unrolling + E-RAFT. This method is similar to the previous method. However, the flow is obtained from E-RAFT [14], which outputs the optical flow between two timestamps t_1 and t_2 , by using events in a window before t_1 and the events between the two timestamps. This method uses a frame and the following events and is therefore closest to our method with respect to the data it uses.

Inpainted Flow unrolling. For both flow unrolling methods, we additionally refine the predictions by training a U-Net to reconstruct the original frames from the intermediate (flow unrolling) predictions. We use different models for the results on `bs_ergb` and `E2D2`, trained on the respective training splits with a learning rate $\lambda = 0.001$, a batchsize of 8 for 100 epochs.

2. Dataset Details

This section presents the single objective beam splitter design and details on E2D2.

2.1. Beam Splitter Design

With the lack of integrated APS pixels (that was a common feature in prior cameras [4, 53]) within recent event based cameras, beam splitters have become common practice to achieve zero baseline images and events [18, 51, 55, 58]. High resolution imagers paired with event based cameras provide the best case scenario for sensor fusion allowing high quality labels such as pixel intensity or semantics. Previous beam splitters constructed for event based camera systems leveraged multiple objective lenses and require a full intrinsic and extrinsic calibration for warping between the imager and event based camera. Mounting a beam splitter after the objective lens allows the sensors to share the same distortion and projection function. We migrate away from c-mount to f-mount lenses in order to achieve the flange distance required to fit a beam splitter cube into the optical path. Figure 10 shows the physical layout of the beam splitter system. The distance between the flange and sensors are the critical distance: comprised of the distance between the sensors and the beam splitter as well as the distance from the beam splitter to the flange. Our system was 3D printed and adjusted for the printer to achieve the ideal back focus.

2.2. Dataset Design

We collect data from the beam splitter with CoCapture [16, 51]. The raw data was temporally aligned using a trigger signal provided by a micro-controller. We calculate the



Figure 10. Constructed single objective beam splitter with each major component labeled. As constructed the Event Camera will be flipped compared to a traditional setup.

Brand	Model	Qty
ThorLabs	CCM1-BS013	1
CenturyArks	SilkyEvVGA	1
FLIR	Chameleon 3	1
Opteka	6mm F-Mount Lens	1
	C to F Mount Adapter	1
	M2 Threaded Insert	12

Table 3. Beam splitter bill of materials

frame timestamps as the time of the trigger events plus half of the exposure time. We follow [35] for the camera calibration. A set of matching corner points is extracted from pairs of images and event intensity images (from `e2vid` [42]). The set of matching corner points is used to directly determine the homography matrix by minimizing the reprojection error between the two domains. Using the calibration, the frames are warped into the event domain.

Our dataset is divided into training, validation, and testing by recording. It is curated such that all frames in the three main parts (training, validation, testing) have sharp frames without motion blur. This is important for training as well as quantification of reconstruction errors. However, event-based cameras are able to operate in regimes that frame-based cameras cannot. To this end, we provide an additional set of sequences for qualitative comparison only. These recordings contain challenging scenarios, where only a small subset of the frames is sharp and the rest underlies heavy motion blur. The subset contains recordings for the downstream tasks novel-view synthesis and tag detection that were shown in 4.2 and further examples for human-pose estimation and rapid camera motion. These additional performance categories provide information on where methods excel and fail.

We will release all full raw sequences in addition to the calibrated and aligned data for future work at the highest quality and with the greatest flexibility. The structure of the raw data will not include a data split as the split we have chosen is optimal for reconstruction purposes, but not necessarily for all tasks.

References

- [1] Patrick Bardow, Andrew J Davison, and Stefan Leutenegger. Simultaneous optical flow and intensity estimation from an event camera. In *Proceedings of the IEEE conference on computer vision and pattern recognition*, pages 884–892, 2016. 3
- [2] Ryad Benosman, Sio-Hoi Ieng, Charles Clercq, Chiara Bartolozzi, and Mandyam Srinivasan. Asynchronous frameless event-based optical flow. *Neural Networks*, 27:32–37, 2012. 3
- [3] Ryad Benosman, Charles Clercq, Xavier Lagorce, Sio-Hoi Ieng, and Chiara Bartolozzi. Event-based visual flow. *IEEE Trans. Neural Netw. Learn. Syst.*, 25(2):407–417, 2013. 3
- [4] Christian Brandli, Raphael Berner, Minhao Yang, Shih-Chii Liu, and Tobi Delbruck. A 240×180 130 db $3 \mu\text{s}$ latency global shutter spatiotemporal vision sensor. *IEEE Journal of Solid-State Circuits*, 49(10):2333–2341, 2014. 12
- [5] Christian Brandli, Lorenz Muller, and Tobi Delbruck. Real-time, high-speed video decomposition using a frame- and event-based davis sensor. In *IEEE Int. Symp. Circuits Syst. (ISCAS)*, pages 686–689, 2014. 2
- [6] Yakun Chang, Chu Zhou, Yuchen Hong, Liwen Hu, Chao Xu, Tiejun Huang, and Boxin Shi. 1000 fps hdr video with a spike-rgb hybrid camera. In *Proceedings of the IEEE/CVF Conference on Computer Vision and Pattern Recognition*, pages 22180–22190, 2023. 4
- [7] Xianhang Cheng and Zhenzhong Chen. Video frame interpolation via deformable separable convolution. In *Proceedings of the AAAI Conference on Artificial Intelligence*, pages 10607–10614, 2020. 2
- [8] A. Dosovitskiy, P. Fischer, E. Ilg, P. Häusser, C. Hazırbaş, V. Golkov, P. v.d. Smagt, D. Cremers, and T. Brox. FlowNet: Learning optical flow with convolutional networks. In *ICCV*, 2015. 6
- [9] Hadar Cohen Duwek, Albert Shalumov, and Elishai Ezra Tsur. Image reconstruction from neuromorphic event cameras using laplacian-prediction and poisson integration with spiking and artificial neural networks. In *Proceedings of the IEEE/CVF Conference on Computer Vision and Pattern Recognition*, pages 1333–1341, 2021. 4
- [10] Yuki Endo, Yoshihiro Kanamori, and Shigeru Kuriyama. Animating landscape: self-supervised learning of decoupled motion and appearance for single-image video synthesis. *arXiv preprint arXiv:1910.07192*, 2019. 3
- [11] Sara Fridovich-Keil, Giacomo Meanti, Frederik Rahbæk Warburg, Benjamin Recht, and Angjoo Kanazawa. K-planes: Explicit radiance fields in space, time, and appearance. In *CVPR*, pages 12479–12488, 2023. 6
- [12] Guillermo Gallego, Henri Rebecq, and Davide Scaramuzza. A unifying contrast maximization framework for event cameras, with applications to motion, depth, and optical flow estimation. In *CVPR*, pages 3867–3876, 2018. 3
- [13] Daniel Gehrig, Mathias Gehrig, Javier Hidalgo-Carrió, and Davide Scaramuzza. Video to events: Recycling video datasets for event cameras. In *CVPR*, 2020. 5
- [14] Mathias Gehrig, Mario Millhäusler, Daniel Gehrig, and Davide Scaramuzza. E-raft: Dense optical flow from event cameras. In *Int. Conf. 3D Vision (3DV)*, pages 197–206. IEEE, 2021. 3, 8, 12
- [15] Mathias Gehrig, Manasi Muglikar, and Davide Scaramuzza. Dense continuous-time optical flow from events and frames. *arXiv preprint arXiv:2203.13674*, 2022. 3
- [16] Friedhelm Hamann and Guillermo Gallego. Stereo co-capture system for recording and tracking fish with frame- and event cameras. *26th Int. Conf. Pattern Recognition (ICPR), Visual observation and analysis of Vertebrate And Insect Behavior (VAIB) Workshop*, 2022. 12
- [17] Zekun Hao, Xun Huang, and Serge Belongie. Controllable video generation with sparse trajectories. In *CVPR*, pages 7854–7863, 2018. 3
- [18] Javier Hidalgo-Carrió, Guillermo Gallego, and Davide Scaramuzza. Event-aided direct sparse odometry. In *Proceedings of the IEEE/CVF Conference on Computer Vision and Pattern Recognition*, pages 5781–5790, 2022. 12
- [19] Aleksander Holynski, Brian L Curless, Steven M Seitz, and Richard Szeliski. Animating pictures with eulerian motion fields. In *Proceedings of the IEEE/CVF Conference on Computer Vision and Pattern Recognition*, pages 5810–5819, 2021. 3
- [20] Xiaotao Hu, Zhewei Huang, Ailin Huang, Jun Xu, and Shuchang Zhou. A dynamic multi-scale voxel flow network for video prediction. In *Proceedings of the IEEE/CVF Conference on Computer Vision and Pattern Recognition*, pages 6121–6131, 2023. 3, 5, 6, 7, 8, 11
- [21] Tiejun Huang, Yajing Zheng, Zhaofei Yu, Rui Chen, Yuan Li, Ruiqin Xiong, Lei Ma, Junwei Zhao, Siwei Dong, Lin Zhu, et al. 1000× faster camera and machine vision with ordinary devices. *Engineering*, 25:110–119, 2023. 4
- [22] Justin Johnson, Alexandre Alahi, and Li Fei-Fei. Perceptual losses for real-time style transfer and super-resolution. In *Computer Vision—ECCV 2016: 14th European Conference, Amsterdam, The Netherlands, October 11–14, 2016, Proceedings, Part II 14*, pages 694–711. Springer, 2016. 7
- [23] Tarun Kalluri, Deepak Pathak, Manmohan Chandraker, and Du Tran. Flavr: Flow-agnostic video representations for fast frame interpolation. In *Proceedings of the IEEE/CVF Winter Conference on Applications of Computer Vision*, pages 2071–2082, 2023. 2
- [24] Bernhard Kerbl, Georgios Kopanas, Thomas Leimkühler, and George Drettakis. 3d gaussian splatting for real-time radiance field rendering. *ACM Transactions on Graphics*, 42(4), 2023. 8
- [25] Hanme Kim, Ankur Handa, Ryad Benosman, Sio-Hoi Ieng, and Andrew J Davison. Simultaneous mosaicing and tracking with an event camera. *J. Solid State Circ.*, 43:566–576, 2008. 3
- [26] Alex X Lee, Richard Zhang, Frederik Ebert, Pieter Abbeel, Chelsea Finn, and Sergey Levine. Stochastic adversarial video prediction. *arXiv preprint arXiv:1804.01523*, 2018. 2
- [27] Hyeongmin Lee, Taeoh Kim, Tae-young Chung, Daehyun Pak, Yuseok Ban, and Sangyoun Lee. Adacof: Adaptive collaboration of flows for video frame interpolation. In *Proceedings of the IEEE/CVF Conference on Computer Vision and Pattern Recognition*, pages 5316–5325, 2020. 2

- [28] Zhengqi Li, Richard Tucker, Noah Snavely, and Aleksander Holynski. Generative image dynamics. *arXiv preprint arXiv:2309.07906*, 2023. [3](#), [4](#)
- [29] Zhengqi Li, Qianqian Wang, Forrester Cole, Richard Tucker, and Noah Snavely. Dynibar: Neural dynamic image-based rendering. In *Proceedings of the IEEE/CVF Conference on Computer Vision and Pattern Recognition*, pages 4273–4284, 2023. [4](#)
- [30] Ziwei Liu, Raymond A Yeh, Xiaoou Tang, Yiming Liu, and Aseem Agarwala. Video frame synthesis using deep voxel flow. In *Proceedings of the IEEE international conference on computer vision*, pages 4463–4471, 2017. [2](#)
- [31] William Lotter, Gabriel Kreiman, and David Cox. Deep predictive coding networks for video prediction and unsupervised learning. *arXiv preprint arXiv:1605.08104*, 2016. [2](#)
- [32] Jérôme Maye, Paul Furgale, and Roland Siegwart. Self-supervised calibration for robotic systems. In *2013 IEEE Intelligent Vehicles Symposium (IV)*, pages 473–480. IEEE, 2013. [8](#)
- [33] N. Mayer, E. Ilg, P. Häusser, P. Fischer, D. Cremers, A. Dosovitskiy, and T. Brox. A large dataset to train convolutional networks for disparity, optical flow, and scene flow estimation. In *IEEE International Conference on Computer Vision and Pattern Recognition (CVPR)*, 2016. [arXiv:1512.02134](#). [6](#)
- [34] Elias Mueggler, Henri Rebecq, Guillermo Gallego, Tobi Delbruck, and Davide Scaramuzza. The event-camera dataset and simulator: Event-based data for pose estimation, visual odometry, and SLAM. *Int. J. Robot. Research*, 36(2):142–149, 2017. [5](#)
- [35] Manasi Muglikar, Mathias Gehrig, Daniel Gehrig, and Davide Scaramuzza. How to calibrate your event camera. In *Proceedings of the IEEE/CVF Conference on Computer Vision and Pattern Recognition*, pages 1403–1409, 2021. [12](#)
- [36] Simon Niklaus and Feng Liu. Softmax splatting for video frame interpolation. In *Proceedings of the IEEE/CVF Conference on Computer Vision and Pattern Recognition*, pages 5437–5446, 2020. [7](#)
- [37] Simon Niklaus, Ping Hu, and Jiawen Chen. Splatting-based synthesis for video frame interpolation. In *Proceedings of the IEEE/CVF Winter Conference on Applications of Computer Vision*, pages 713–723, 2023. [2](#)
- [38] Edwin Olson. Apriltag: A robust and flexible visual fiducial system. In *2011 IEEE international conference on robotics and automation*, pages 3400–3407. IEEE, 2011. [8](#)
- [39] Bernd Pfrommer. Frequency cam: Imaging periodic signals in real-time. *arXiv preprint arXiv:2211.00198*, 2022. [5](#)
- [40] Bernd Pfrommer and Kostas Daniilidis. Tagslam: Robust slam with fiducial markers. *arXiv preprint arXiv:1910.00679*, 2019. [8](#)
- [41] Henri Rebecq, René Ranftl, Vladlen Koltun, and Davide Scaramuzza. Events-to-video: Bringing modern computer vision to event cameras. In *Proceedings of the IEEE/CVF Conference on Computer Vision and Pattern Recognition*, pages 3857–3866, 2019. [4](#)
- [42] Henri Rebecq, René Ranftl, Vladlen Koltun, and Davide Scaramuzza. High speed and high dynamic range video with an event camera. *IEEE transactions on pattern analysis and machine intelligence*, 43(6):1964–1980, 2019. [4](#), [12](#)
- [43] Fitsum Reda, Janne Kontkanen, Eric Tabellion, Deqing Sun, Caroline Pantofaru, and Brian Curless. Film: Frame interpolation for large motion. In *European Conference on Computer Vision*, pages 250–266. Springer, 2022. [2](#), [3](#), [5](#), [6](#), [7](#), [8](#), [10](#), [11](#)
- [44] Viktor Rudnev, Mohamed Elgharib, Christian Theobalt, and Vladislav Golyanik. Eventnerf: Neural radiance fields from a single colour event camera. In *CVPR*, pages 4992–5002, 2023. [5](#)
- [45] Cedric Scheerlinck, Nick Barnes, and Robert Mahony. Continuous-time intensity estimation using event cameras. In *ACCV*, pages 308–324, 2018. [3](#), [4](#), [5](#)
- [46] Cedric Scheerlinck, Henri Rebecq, Daniel Gehrig, Nick Barnes, Robert Mahony, and Davide Scaramuzza. Fast image reconstruction with an event camera. In *Proceedings of the IEEE/CVF Winter Conference on Applications of Computer Vision*, pages 156–163, 2020. [4](#)
- [47] Johannes Lutz Schönberger and Jan-Michael Frahm. Structure-from-motion revisited. In *Conference on Computer Vision and Pattern Recognition (CVPR)*, 2016. [8](#)
- [48] Johannes Lutz Schönberger, Enliang Zheng, Marc Pollefeys, and Jan-Michael Frahm. Pixelwise view selection for unstructured multi-view stereo. In *European Conference on Computer Vision (ECCV)*, 2016. [8](#)
- [49] Shintaro Shiba, Yoshimitsu Aoki, and Guillermo Gallego. Event collapse in contrast maximization frameworks. *Sensors*, 22(14):5190, 2022. [3](#)
- [50] Shintaro Shiba, Yoshimitsu Aoki, and Guillermo Gallego. Secrets of event-based optical flow. In *ECCV*, pages 628–645. Springer, 2022. [3](#)
- [51] Shintaro Shiba, Friedhelm Hamann, Yoshimitsu Aoki, and Guillermo Gallego. Event-based background-oriented schlieren. *IEEE Transactions on Pattern Analysis and Machine Intelligence*, 2023. [12](#)
- [52] Timo Stoffregen, Guillermo Gallego, Tom Drummond, Lindsay Kleeman, and Davide Scaramuzza. Event-based motion segmentation by motion compensation. In *ICCV*, pages 7244–7253, 2019. [3](#)
- [53] Gemma Taverni, Diederik Paul Moeys, Chenghan Li, Celso Cavaco, Vasyl Motsnyi, David San Segundo Bello, and Tobi Delbruck. Front and back illuminated dynamic and active pixel vision sensors comparison. *IEEE Transactions on Circuits and Systems II: Express Briefs*, 65(5):677–681, 2018. [12](#)
- [54] Zachary Teed and Jia Deng. Raft: Recurrent all-pairs field transforms for optical flow. In *ECCV*, pages 402–419. Springer, 2020. [6](#), [7](#), [8](#), [12](#)
- [55] Stepan Tulyakov, Daniel Gehrig, Stamatios Georgoulis, Julius Erbach, Mathias Gehrig, Yuanyou Li, and Davide Scaramuzza. TimeLens: Event-based video frame interpolation. *CVPR*, 2021. [2](#), [6](#), [7](#), [12](#)
- [56] Stepan Tulyakov, Alfredo Bochicchio, Daniel Gehrig, Stamatios Georgoulis, Yuanyou Li, and Davide Scaramuzza. Time lens++: Event-based frame interpolation with parametric non-linear flow and multi-scale fusion. In *CVPR*, pages 17755–17764, 2022. [2](#), [3](#), [5](#), [6](#), [7](#), [8](#)

- [57] Chaoyang Wang, Ben Eckart, Simon Lucey, and Orazio Gallo. Neural trajectory fields for dynamic novel view synthesis. *arXiv preprint arXiv:2105.05994*, 2021. 4
- [58] Zihao W Wang, Peiqi Duan, Oliver Cossairt, Aggelos Kat-saggelos, Tiejun Huang, and Boxin Shi. Joint filtering of in-tensity images and neuromorphic events for high-resolution noise-robust imaging. In *Proceedings of the IEEE/CVF Con-ference on Computer Vision and Pattern Recognition*, pages 1609–1619, 2020. 12
- [59] Wenming Weng, Yueyi Zhang, and Zhiwei Xiong. Event-based video reconstruction using transformer. In *Proceed-ings of the IEEE/CVF International Conference on Com-puter Vision*, pages 2563–2572, 2021. 4
- [60] Tianfan Xue, Jiajun Wu, Katherine Bouman, and Bill Free-man. Visual dynamics: Probabilistic future frame synthesis via cross convolutional networks. *Advances in neural infor-mation processing systems*, 29, 2016. 2
- [61] Yixin Yang, Jin Han, Jinxiu Liang, Imari Sato, and Boxin Shi. Learning event guided high dynamic range video re-construction. In *Proceedings of the IEEE/CVF Conference on Computer Vision and Pattern Recognition*, pages 13924–13934, 2023. 4
- [62] Chengxi Ye, Anton Mitrokhin, Cornelia Fermüller, James A Yorke, and Yiannis Aloimonos. Unsupervised learning of dense optical flow, depth and egomotion with event-based sensors. In *2020 IEEE/RSJ International Conference on Intelligent Robots and Systems (IROS)*, pages 5831–5838. IEEE, 2020. 3
- [63] Richard Zhang, Phillip Isola, Alexei A Efros, Eli Shecht-man, and Oliver Wang. The unreasonable effectiveness of deep features as a perceptual metric. In *Proceedings of the IEEE conference on computer vision and pattern recogni-tion*, pages 586–595, 2018. 7
- [64] Zelin Zhang, Anthony Yezzi, and Guillermo Gallego. For-mulating event-based image reconstruction as a linear in-verse problem with deep regularization using optical flow. *arXiv preprint arXiv:2112.06242*, 2021. 4
- [65] Alex Zihao Zhu, Yibo Chen, and Kostas Daniilidis. Realtime time synchronized event-based stereo. In *ECCV*, pages 433–447, 2018. 3
- [66] Alex Zihao Zhu, Liangzhe Yuan, Kenneth Chaney, and Kostas Daniilidis. Ev-flownet: Self-supervised optical flow estimation for event-based cameras. *arXiv preprint arXiv:1802.06898*, 2018. 3, 7, 11
- [67] Alex Zihao Zhu, Liangzhe Yuan, Kenneth Chaney, and Kostas Daniilidis. Unsupervised event-based learning of op-tical flow, depth, and egomotion. In *CVPR*, pages 989–997, 2019. 3